Biochem. J. (2013) **454**, 239–247 (Printed in Great Britain) doi:10.1042/BJ20130415

Cross-functionalities of *Bacillus* deacetylases involved in bacillithiol biosynthesis and bacillithiol-S-conjugate detoxification pathways

Zhong FANG*, Alexandra A. ROBERTS†, Karissa WEIDMAN*, Sunil V. SHARMA†, Al CLAIBORNE‡, Christopher J. HAMILTON† and Patricia C. DOS SANTOS*[1]

*Department of Chemistry, Wake Forest University, Winston-Salem, NC 27109, U.S.A., †School of Pharmacy, University of East Anglia, Norwich Research Park, Norwich NR4 7TJ, U.K., and ‡Center for Structural Biology, Wake Forest University School of Medicine, Winston-Salem, NC 27109, U.S.A.

BshB, a key enzyme in bacillithiol biosynthesis, hydrolyses the acetyl group from *N*-acetylglucosamine malate to generate glucosamine malate. In *Bacillus anthracis*, BA1557 has been identified as the *N*-acetylglucosamine malate deacetylase (BshB); however, a high content of bacillithiol (~70%) was still observed in the *B. anthracis* Δ*BA1557* strain. Genomic analysis led to the proposal that another deacetylase could exhibit cross-functionality in bacillithiol biosynthesis. In the present study, BA1557, its paralogue BA3888 and orthologous *Bacillus cereus* enzymes BC1534 and BC3461 have been characterized for their deacetylase activity towards *N*-acetylglucosamine malate, thus providing biochemical evidence for this proposal. In addition, the involvement of deacetylase enzymes is also expected in bacillithiol-detoxifying pathways through formation of S-mercapturic adducts. The kinetic analysis of bacillithiol-S-bimane conjugate favours the involvement of BA3888 as the *B. anthracis* bacillithiol-S-conjugate amidase (Bca). The high degree of specificity of this group of enzymes for its physiological substrate, along with their similar pH–activity profile and Zn^{2+}-dependent catalytic acid–base reaction provides further evidence for their cross-functionalities.

Key words: bacillithiol, bimane, BshB, deacetylase, *N*-acetylglucosamine malate, zinc hydrolase.

INTRODUCTION

The cysteine-containing tripeptide glutathione (GSH) is the major low-molecular-mass thiol in eukaryotes and many Gram-negative bacteria (Figure 1). In addition to its major role in thiol-redox homoeostasis [1], GSH is also widely implicated in xenobiotic detoxification. This is facilitated by GSTs, which can catalyse S-conjugation of GSH to a diverse range of electrophilic xenobiotics [2]. In Gram-negative bacteria, GSH plays a sacrificial role in electrophile detoxification as these glutathione S-conjugates are directly exported from the cell [3].

Many Gram-positive bacteria lack GSH, but instead produce other low-molecular-mass thiols. Mycothiol (MSH) (Figure 1) is the dominant low-molecular-mass thiol in Actinobacteria (formerly known as Actinomycetes) (e.g. *Mycobacterium*, *Corynebacterium* and *Streptomyces*), which serves functions analogous to those of GSH [4,5]. However, one notable difference is that MSH-dependent drug detoxification pathways utilize a mycothiol-S-conjugate amidase (Mca) to hydrolyse the mycothiol S-conjugate amide linkage to liberate the CysNAc (*N*-acetylcysteine) S-conjugate (mercapturic acid), which is exported from the cell, and glucosamine inositol, which is recycled back into the MSH biosynthetic pathway [6].

In 2009, bacillithiol (BSH) (Figure 1) was identified as a low-molecular-mass thiol among many low-G+C Gram-positive bacteria (Firmicutes) lacking GSH or MSH [7]. These include *Bacillus* spp. (e.g. *B. anthracis*, *B. subtilis*, *B. cereus*, *B. megaterium* and *B. pumilis*) and some, but not all, staphylococci (e.g. *Staphylococcus aureus* and *Staphylococcus saprophyticus*) and streptococci (e.g. *Streptococcus agalactiae*). So far, BSH-deficient mutants have been shown to display impaired sporulation, sensitivity to acid and salt, increased sensitivity to fosfomycin [8] and reduced viability in mouse macrophage cell lines [9]. A detailed understanding of the enzymes mediating BSH biosynthesis and BSH-dependent drug resistance is central to identifying whether and how such biological targets could be exploited for the design of new antibiotic chemotherapies.

The three-step biosynthetic pathway for BSH (Figure 2) shares similarities with the key steps in MSH biosynthesis. BSH biosynthesis is initiated by a retaining glycosyltransferase (BshA) that catalyses the glycosylation of L-malic acid to afford GlcNAc-Mal (*N*-acetylglucosamine malate) [8,10]. An N-acetylhydrolase (BshB) then liberates the free amine GlcN-Mal (glucosamine malate) [8,10]. Gene-knockout studies in *B. subtilis* have identified a bacillithiol synthase (BshC) [8], proposed to catalyse the final conversion of GlcN-Mal into BSH, but attempts to demonstrate the BSH synthase activity of BshC *in vitro* have so far been unsuccessful.

In many bacilli (e.g. *B. subtilis*, *B. anthracis* and *B. cereus*), *bshA* and *bshB* are adjacent genes located in the same operon [8] (Table 1). Whereas BshA and BshC are essential for BSH biosynthesis, in many cases *bshB*-knockout mutants display only a partial reduction in BSH levels [8,10]. This has been attributed to the presence of one, or more, additional *bshB*-like gene products, which can also N-deacetylate GlcNAc-Mal. In *B. subtilis*, for example, a Δ*bshB1* (*ypjG*) mutant retains almost half of the WT (wild-type) levels of BSH, whereas the Δ*bshB1* + Δ*bshB2* (*yojG*) double-knockout strain showed no detectable levels of BSH [8,10]. Although *in vivo* data provide a strong indication

Abbreviations used: Bca, bacillithiol-S-conjugate amidase; BS–Fos, bacillithiol–fosfomycin; BSH, bacillithiol; BSmB, bacillithiol-S-bimane; CysmB, cysteine monobromobimane derivative; DETAPAC, diethylenetriaminepenta-acetic acid; FU, fluorescence unit(s); GlcNAc-Mal, *N*-acetylglucosamine malate; GlcNAc-OBn, *O*-benzyl-*N*-acetylglucosamine; GlcNAc-OMe, *O*-methyl-*N*-acetylglucosamine; GlcN-Mal, glucosamine malate; ICP-AES, inductively coupled plasma atomic emission spectroscopy; IMAC, immobilized metal-ion-affinity chromatography; mBBr, monobromobimane; Mca, mycothiol-S-conjugate amidase; MSH, mycothiol; NDA, naphthalene-2,3-dialdehyde; WT, wild-type.

[1] To whom correspondence should be addressed (email dossanpc@wfu.edu).

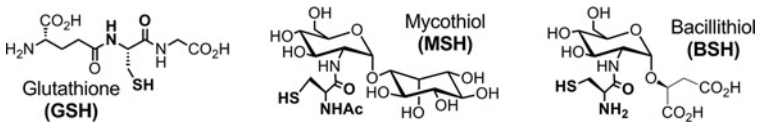

Figure 1 Low-molecular-mass thiols found in bacteria

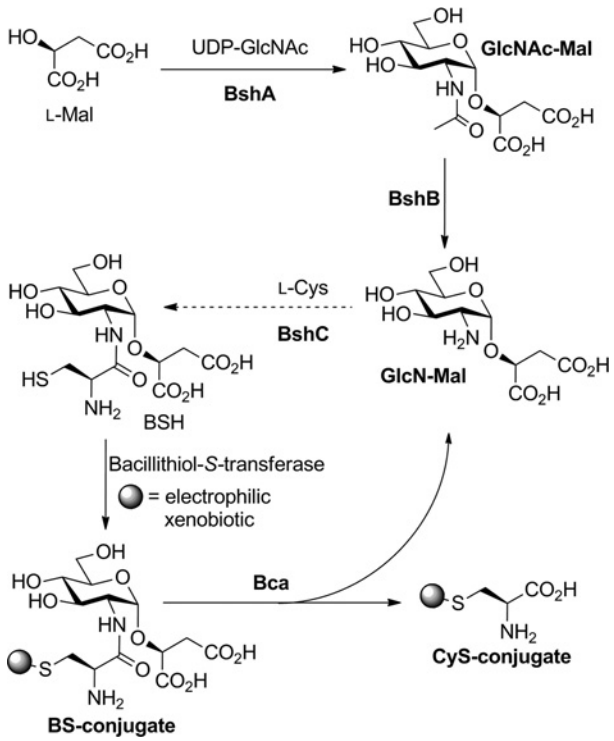

Figure 2 The proposed biosynthetic pathway and detoxification mechanism of bacillithiol

for cross-functionality of BshB and orthologous enzymes in the biosynthesis of bacillithiol, biochemical validation of this proposal has not been carried out. In *Mycobacterium smegmatis*, functional redundancy was also observed for analogous N-deacetylase in MSH biosynthesis (MshB). In this case 5–10 % of WT MSH levels are still produced in Δ*mshB* mutants due to the residing background N-deacetylase activity of Mca [11,12]. Interestingly, in *S. aureus*, which only contains a single *bshB*-like gene, preliminary studies have indicated the presence of a bacillithiol-S-conjugate amidase (Bca) pathway that is capable of detoxifying the electrophilic xenobiotic monobromobimane [13]. Considering these *in vivo* observations, it seems plausible that one or more of these BshB-like enzymes could also present Bca activity in xenobiotic detoxification. In pathways involving BSH, neither the identity of any Bca enzyme (the equivalent of Mca in BSH-producing species) nor the kinetic analysis of enzymes able to perform both reactions has been determined.

Before the discovery of BSH, the crystal structure of a *B. cereus* Zn^{2+}-binding protein (BC1534) (shown in the present study to be a BshB) was reported [14,15], which was characterized as a potential chitin deacetylase on the basis of its observed N-deacetylase activity with GlcNAc (K_m, 3 μM; k_{cat}, 2 s^{-1}) and chitobiose (K_m, 3 μM; k_{cat}, 98 s^{-1}) [14,15]. Since then, initial kinetic studies of the homologous (97 % sequence identity) *B. anthracis* enzyme (BA1557) have demonstrated its BshB activity with GlcNAc-Mal, but no notable GlcNAc deacetylase activity was observed [8,10]. Although it is anticipated that GlcNAc-Mal is the physiological substrate of BC1534, the participation of BC1534 and/or BC3461 in BSH biosynthesis and/or detoxification has not been explored at all.

Table 1 Functional assignment of BSH biosynthetic and detoxification genes

Organism	BshA	BshB	Bca/BshB2
B. anthracis	BA1558	BA1557	BA3888
B. cereus	BC1535	BC1534	BC3461
B. subtilis	BSU22460 (ypjH)	BSU22470 (*ypjG*)	BSU19460 (*yojG*)
S. aureus	SA2981_1414	–	SA2981_0544

In the present study, we have investigated the BshB and Bca properties of the *B. anthracis* N-deacetylases BA1557, BA3888 and BA3524 as well as the orthologous *B. cereus* enzymes BC1534 and BC3461 (Table 1). The results indicate that both BA1557 and BA3888 (and the *B. cereus* homologues) are competent in catalysing the N-deacetylation of GlcNAc-Mal, whereas BA3888 showed activity against BSmB (bacillithiol-S-bimane) adduct. Assays with GlcNAc-Mal substrate analogues demonstrate that the malate portion of the molecule plays a role in controlling substrate specificity. In addition, a site-directed mutagenesis approach provides insight into the mechanistic details of the Zn^{2+}-dependent catalytic acid–base reaction.

MATERIALS AND METHODS

Materials

BSmB [16], GlcNAc-Mal [17], GlcNAc-OBn (*O*-benzyl-*N*-acetylglucosamine) [18] and GlcNAc-OMe (*O*-methyl-*N*-acetylglucosamine) [19] were chemically synthesized as described previously. BS–Fos (bacillithiol–fosfomycin) was enzymatically synthesized via FosB-catalysed S-conjugation of BSH with fosfomycin [16]. GlcNAc was purchased from Acros, and NDA (naphthalene-2,3-dialdehyde) was from Anaspec. All other reagents were purchased from Fisher Scientific or Sigma.

Expression and purification of *B. anthracis* BA1557, BA3524 and BA3888, and *B. cereus* BC1534 and BC3461

The cloning of BA1557 (BshB) was described by Parsonage et al. [10]. The codon-optimized genes for BA3524 and BA3888 were synthesized by GenScript and subcloned into pET28a (+) (Novagen). BC1534 in pET26b (+) [15] and BC3461 in pET24a (+) were generously provided by Dr Vassilis Bouriotis and Dr Vasiliki Fadouloglou (both at Department of Biology, University of Crete, Heraklion, Crete, Greece). All variants of BA1557 were prepared using the QuikChange® site-directed mutagenesis kit (Stratagene), and confirmed by DNA sequencing. All proteins used in the present study contained a C-terminal hexahistidine tag.

BA1557, BC1534 and all BA1557 variants were purified using the following general protocol. The plasmid was transformed into

chemically competent *Escherichia coli* BL21(DE3) cells, which were plated on LB plates with 40 μg/ml kanamycin in a 37 °C incubator overnight. For protein expression, 3 litres of LB broth supplemented with 40 μg/ml kanamycin were inoculated with freshly transformed cells and incubated at 37 °C with shaking at 300 rev./min. Expression was induced upon addition of 5.8 mM lactose when the D_{600} reached 0.5, and the culture was incubated further at 15 °C with shaking at 300 rev./min overnight before being harvested by centrifugation at 5000 ***g*** for 10 min at 4 °C. The cells were stored at − 20 °C until further use. Cells were resuspended with 25 mM Tris/HCl (pH 8.0), 150 mM NaCl and 10 % glycerol (buffer A), and then lysed using an EmulsiFlex-C5 high-pressure homogenizer. The cell debris was separated by centrifugation at 12000 ***g*** for 30 min, and the supernatant was cleared upon treatment with 1 % (w/v) streptomycin sulfate followed by centrifugation at 12000 ***g*** for 20 min. After the treatment, the clear supernatant was loaded on to pre-equilibrated (buffer A) Zn^{2+}- or Co^{2+}-IMAC (immobilized metal-ion-affinity chromatography) columns (GE Healthcare). The column was washed with buffer A until the A_{280} reached baseline. Proteins associated with the resin were eluted in a step gradient of 5 %, 15 % and 50 % of buffer B (25 mM Tris/HCl, pH 8.0, 150 mM NaCl, 300 mM imidazole and 10 % glycerol). The fractions eluted from 50 % of buffer B containing pure proteins were diluted five times with buffer C (25 mM Tris/HCl, pH 8.0 and 10 % glycerol), and loaded on to a 5 ml Hitrap Q FF (GE Healthcare) column pre-equilibrated with buffer C. The desired protein was eluted with 0.5 M NaCl in the same buffer. Protein concentration was determined by the Bradford assay using BSA as the standard [20]. Protein aliquots were frozen with liquid nitrogen and stored at − 80 °C.

Because of the poor solubility experienced with BA3888 in pET vector expression, the gene was subcloned into the pBAD vector. The purification of pBAD-BA3888 and pET24a-BC3461 used the same procedure. The plasmids were transformed into *E. coli* BL21(DE3) cells, and cells were plated on LB agar with 100 μg/ml ampicillin or 40 μg/ml kanamycin. The inoculum was prepared with several colonies taken from a plate and transferred into 100 ml of LB broth with appropriate antibiotics. After 1 h of incubation at 37 °C with shaking at 300 rev./min, the inoculum was added to 4 litres of LB broth with antibiotics and incubated at 37 °C with shaking at 300 rev./min. Protein expression was induced at a D_{600} of 0.4 by the addition of 5.8 mM lactose or 20 mM arabinose (final concentrations). The culture was shaken at 37 °C for another 4 h before being harvested by centrifugation. The cells were lysed as described above, and the soluble proteins were loaded on to a nickel-IMAC column pre-equilibrated with buffer A. The column was washed with buffer A, and proteins associated with the column were eluted with a step gradient (5 %, 15 %, 30 %, 50 % and 100 %) of buffer B. Fractions containing deacetylase activity were pooled, diluted 6-fold with 25 mM Hepes (pH 8.0) and 10 % glycerol (buffer D), and loaded on to a MonoQ column (GE Healthcare) equilibrated with buffer D. Proteins associated with the column were eluted in a 20 ml linear gradient from 0 to 0.75 M NaCl in buffer D. Pure protein fractions (by SDS/PAGE) containing activity were combined and aliquots of 20 μl were then frozen in liquid nitrogen for storage at − 80 °C. Within 10 days of the purification date, freshly thawed aliquots were used for kinetic experiments.

CD spectroscopy

CD spectra were obtained using an Aviv CD spectrometer (Model 215; AVIV Biomedical) with a 1-mm-pathlength quartz cuvette (Hellma Analytics) and a bandwidth of 1 nm. Protein samples were analysed at 5 μM in 10 mM phosphate buffer (pH 7.4) and scanned from 250 nm to 190 nm with 0.5 nm increments. The final spectrum of each sample is the average of ten scans.

Enzyme assays for N-deacetylation of GlcNAc-Mal, GlcNAc-OBn, GlcNAc-OMe and GlcNAc

The deacetylation activity was assayed by quantification of the primary amine product. In general, a 200 μl assay mixture containing 50 mM Mops (pH 7.4) and 0.1–20 μg of enzyme was pre-equilibrated at 37 °C for 5 min. Reactions were initiated by the addition of substrate. Sample aliquots (20 μl) were taken at different time points and quenched with 20 μl of acetonitrile. The primary amine products (GlcN, GlcN-Mal, etc.) were then derivatized by addition of 200 μl of freshly prepared NDA-mix (0.4 M borate, pH 9, 2.5 mM KCN and 0.5 mM NDA). The solution mixture was allowed to react in the dark for 30 min before being read in a flat-bottom microplate (Costar) using a Synergy H1 plate reader (Biotek) with λ_{ex} 390 nm and λ_{em} 480 nm. Initial velocity was determined from the slope of a plot of FU (fluorescence units) against time using four different time points over a period of up to 3 h. A glucosamine standard curve was used to convert the FU/min slopes into [product]/min; the fluorescence intensity of the GlcN–NDA product was identical with that of the GlcN-Mal–NDA. Initial deacetylation rates of GlcNAc-Mal were measured over the concentration range 0–3.5 mM. For determination of the steady-state parameters, results representing the means of triplicate values were fitted to the Michaelis–Menten equation using SigmaPlot 11.0.

Enzyme assays for amidase activity with BSmB, BSH and BS–Fos

Amidase activity of BSH was assayed by quantification of the mBBr (monobromobimane) derivative of cysteine (CysmB) produced during hydrolysis of BSmB. A representative assay contained 1.5–20 μg of enzyme in 200 μl of 50 mM Mops (pH 7.4) pre-warmed at 37 °C for 5 min. The reaction was initiated by addition of BSmB. After incubation for various time intervals, reaction aliquots (10 μl) were quenched by the addition of 20 μl of acetonitrile followed by centrifugation (5 min). The supernatant (20 μl) was diluted 50-fold with 5 mM HCl before analysis by HPLC using procedures described previously [7].

The amidase activity towards BSH was assayed by quantification of cysteine formation by derivatization of the thiol with mBBr. The assay was performed by first equilibrating 40 μM of the enzyme in 50 mM Hepes buffer (pH 7.4) for 10 min at 37 °C. The reactions were initiated upon addition of substrate (0.2–10 mM BSH) followed by incubation for 30 min at 37 °C. Aliquots of 10 μl were collected at various time points and the reaction was quenched by heating at 80 °C for 10 min. Reaction aliquots (4 μl) were then derivatized with 6 μl of 100 mM mBBr for 15 min at room temperature (25 °C) to label the cysteine product and quenched upon addition of 0.25 μl of 5 M methanesulfonic acid and centrifuged at 10000 ***g*** for 5 min. Finally, the supernatant was diluted with 100 μl of 10 mM methanesulfonic acid and 50 μl of sample was analysed by HPLC as described previously [7]. The activities were calculated from a calibration curve using CysmB as the standard. The means of three duplicates were fitted into the Michaelis–Menten equation to determine the steady-state parameters.

The activity towards BS–Fos was assayed by quantifying cysteine–fosfomycin and GlcN-Mal using the AccQ Fluor reagent kit (Waters) to detect the primary amine products. A solution containing 40 μM of enzyme in 50 mM Hepes (pH 7.4) was pre-warmed at 37 °C for 5 min and the reaction was started

upon addition of 0.5 mM BS–Fos. After 30 min, reactions were quenched by heating the samples at 85 °C for 10 min. The derivation of amine products with AccQ Fluor reagent was performed as recommended by the manufacture. The samples were assayed via HPLC as described previously [21].

Preparation of metal-free deacetylase and metal reconstitution

To prepare metal-free BA1557, Co^{2+}-IMAC-purified protein (~75 μM) was incubated with 25 mM Tris/HCl (pH 7.5), 25 mM DETAPAC (diethylenetriaminepenta-acetic acid) and 10 % glycerol on ice for 30 min. The protein solution was then dialysed three times over 2 litres of 25 mM Tris/HCl (pH 7.5) and 10 % glycerol buffer at 4 °C. The concentration of residual metal ion was determined to be less than 5 % by ICP-AES (inductively coupled plasma atomic emission spectroscopy) (Tedeyne Leeman Labs) analysis.

For the reconstitution with Zn^{2+}, apo-BA1557 (10 μM) was incubated with different stoichiometric ratios of $ZnSO_4$ on ice for 30 min. The solution was then dialysed against 1 litre of 25 mM Tris/HCl (pH 8.0) and 10 % glycerol at 4 °C to remove unbound Zn^{2+}, and the protein metal content was measured by ICP-AES.

pH-dependent activity profiles

For the pH-dependence experiments, the following buffers were used: 50 mM Mes (pH 6.0–7.0); 50 mM Mops (pH 7.0–8.0); 50 mM bicine (pH 8.0–9.0); and 50 mM borate (pH 9.0–10.0). The standard assay protocol was conducted by equilibrating 200 μl of buffer containing 0.4 μg of deacetylase at 37 °C. The deacetylation reaction was initiated by the addition of 0.25 mM GlcNAc-Mal. Samples (20 μl) were taken at intervals, and the reaction was terminated by addition of an equal volume of acetonitrile. Steady-state kinetic parameters K_m, k_{cat} and k_{cat}/K_m for deacetylase activity were determined by fitting initial velocities to the Michaelis–Menten equation. Eqn (1) was fitted to the pH rate profile, wherein V is the observed rate of the reaction, K is the pH-independent rate constant for GlcNAc or GlcNAc-Mal substrates, and K_a and K_b are the ionization constants of the acid and base species respectively [22]:

$$V/K = \frac{1}{1 + 10^{-pH}/K_a + K_b/10^{-pH}} \quad (1)$$

RESULTS

Cross-functionality of deacetylases in BshB catalysis

Previous work described the ability of BA1557 to catalyse the hydrolysis of GlcNAc-Mal using an assay that involved HPLC analysis of GlcN-Mal product formation after derivatization with the amine-specific fluorophore (AccQ tag) [10]. In the present study, BA1557 and other BshB-like enzymes have been extensively characterized through the application of a faster assay procedure that bypasses the need to quantify derivatized reaction products by HPLC separation. This was achieved by developing a fluorescence microplate assay to detect GlcN-Mal formation following derivatization of the secondary amine with NDA [23]. This method is more cost-effective and faster than the commercial AccQ tag kit [10], and is ~50-fold more sensitive than methods involving a direct fluorescamine-based procedure [24]. Despite the aforementioned benefits of this method, NDA-derivatization of primary amines is not specific to the deacetylation product and background signal associated with other primary amines present in the reaction mixture is a recurring limitation of such amine-specific fluorescence-based assays [25]. Nevertheless, the high sensitivity of this method allowed us to optimize the use of synthetic substrates (Table 2 and Figure 3), many of which were only available in limited quantities.

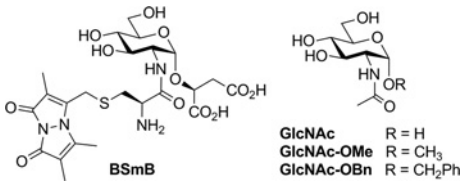

Figure 3 Structures of substrates included in Table 2

Ph, phenyl.

Table 2 Substrate specificity of *B. anthracis* and *B. cereus* N-deacetylases

All assays were performed in the presence of 5 mM substrate with 0.23–6.25 μM enzyme, except for GlcNAc-Mal, which was assayed in the presence of 0.5 mM substrate with 0.033–1.05 μM enzyme.

	Specific activity (nmol/min per mg)			
Substrate	BA1557	BC1534	BA3888	BC3461
GlcNAc	0.55 ± 0.01	0.87 ± 0.12	<0.05	0.46 ± 0.025
GlcNAc-OMe	<0.05	<0.05	4.55 ± 0.32	0.8 ± 0.02
GlcNAc-OBn	2.00 ± 0.04	1.90 ± 0.02	<0.05	0.36 ± 0.02
GlcNAc-Mal	14227 ± 192	17705 ± 207	8430 ± 490	10.7 ± 0.3
BSmB	0.363 + 0.058	0.226	73.7 ± 7.9	0.4 ± 0.05
BSH	1.3	0.7	2.58	1.1

The activity of BA1557 with GlcNAc-Mal (19 ± 1.1 μmol/min per mg), when tested using this method, was comparable with that obtained with the AccQ tag (21.5 ± 0.2 μmol/min per mg) or fluorescamine procedures (19.8 ± 1.0 μmol/min per mg). BA3888 also displayed comparable substrate kinetics with those of GlcNAc-Mal, thereby demonstrating the functional redundancy of BA1557 in the second step of BSH biosynthesis (Table 3 and Supplementary Figure S1A at http://www.biochemj.org/bj/454/bj4540239add.htm). The kinetic analysis of both enzymes fits well with the *in vivo* data, which demonstrated a 70 % reduction in BSH levels in the *B. anthracis* Δ*bshB* strain [10]. As expected, the orthologous BC1534 (97 % sequence identity) displays very similar kinetic behaviour in the BshB reaction (Table 3 and Supplementary Figure S1A), supporting the proposed role for this enzyme in the biosynthesis of BSH. The catalytic efficiencies (k_{cat}/K_m) of BA1557 and BC1534 with GlcNAc were four orders of magnitude lower than that determined against GlcNAc-Mal, whereas BA3888 showed no detectable activity (Table 3 and Supplementary Figure S1A). The calculated k_{cat}/K_m values for BA1557 and BC1534 with GlcNAc were substantially (six orders of magnitude) lower than the values reported previously for the *B. cereus* enzyme [15], but similar to the values reported for *B. anthracis* [10].

Additional N-deacetylase candidates, BA3524 and BC3461, were investigated in the BshB reaction. The two enzymes are 95 % identical in sequence and are likely to perform similar intracellular functions (Supplementary Figure S2B at http://www.biochemj.org/bj/454/bj4540239add.htm). Phylogenetic analysis shows that they constitute a separate branch of N-acetylhydrolases, different from those including BA1557 or BA3888 (Supplementary Figure S3 at http://www.biochemj.org/bj/454/bj4540239add.htm). In our hands, BC3461 showed limited activity with GlcNAc-Mal

Table 3 Kinetic parameters of *B. anthracis* and *B. cereus* N-deacetylases

ND, not determined.

Enzyme	Substrate	K_m (mM)	k_{cat} (s^{-1})	k_{cat}/K_m ($s^{-1}\cdot M^{-1}$)	Reference
BA1557	GlcNAc-Mal	0.19 ± 0.03	8.24 ± 0.46	43300 ± 7300	The present study
	GlcNAc-Mal	0.16	42	262000	[9]
	GlcNAc	57.1 ± 8.5	$(3.3 \pm 0.14)\times10^{-3}$	0.058 ± 0.01	The present study
	GlcNAc	ND	$\sim 8\times10^{-5}$		[9]
	BSH	0.48 ± 0.05	$(7.0 \pm 0.15)\times10^{-4}$	1.4 ± 0.18	The present study
	BSmB	0.32 ± 0.05	$(2.0 \pm 0.10)\times10^{-4}$	0.7 ± 0.13	The present study
BA3888	GlcNAc-Mal	0.32 ± 0.09	6.48 ± 0.66	20300 ± 6000	The present study
	GlcNAc	–*	–*	–*	The present study
	BSH	>5†	$(1.1 \pm 0.14)\times10^{-3}$		The present study
	BSmB	>5†	0.031 ± 0.0033		The present study
BC1534	GlcNAc-Mal	0.20 ± 0.01	10.80 ± 0.22	54000 ± 2900	The present study
	GlcNAc	16.9 ± 1.8	$(2.0 \pm 0.1)\times10^{-3}$	0.12 ± 0.014	The present study
	GlcNAc	0.003	1.89	6.3×10^{5}	[14]
BC3461	GlcNAc-Mal	0.21 ± 0.03	0.068 ± 0.003	320 ± 4.8	The present study
	GlcNAc	–*	–*	–*	The present study
	GlcNAc	0.009	6.4	7.1×10^{5}	[14]

*Activity was not detected when using 1–10 mM substrate.

†Rate against substrate concentration was still in the linear region at the maximum concentration assayed (5 mM); the reaction rate under these conditions was used to calculate turnover rate.

(Table 3), whereas BA3524 displayed no detectable activity. Far-UV CD spectra and ICP-AES analyses of these proteins indicated comparable secondary structure, and Zn^{2+} content with those of BA1557, BA3888 and BC1534 (Supplementary Figure S4 at http://www.biochemj.org/bj/454/bj4540239add.htm). This observation indicates that the lack of activity seems not to be attributed to protein misfolding or lack of metal cofactor resulting from heterologous *E. coli* expression.

Zn^{2+}-dependent deacetylase activity

The Zn^{2+}-binding site identified in the structure of BC1534 (*Bc*ZBP) displayed a similar arrangement to that found in the active sites of other Zn^{2+}-dependent deacetylases [14]. Like the MshB structure, the BC1534 active site displays two histidine residues and one aspartate residue (His^{12}, His^{113} and Asp^{15}) providing a facial triad Zn^{2+} co-ordination [14,26] (Figure 4). All three metal-ion-co-ordinating residues are strictly conserved in the MshB and Mca sequences, in addition to the BshB and Bca candidate enzymes from *B. anthracis* and other BSH-producing species (Supplementary Figure S2). Hexahistidine-tagged recombinant BA1557, purified by Zn^{2+}-affinity chromatography contains 2.55 ± 0.04 Zn^{2+} cations per monomer. Treatment with 20 mM EDTA or EGTA had a minor effect on either metal content or enzyme activity (less than 20 % decrease upon 1 h of incubation), whereas treatment with the stronger metal-chelating reagent DETAPAC removes nearly 98 % of the bound Zn^{2+} and almost completely inactivates the enzyme. This indicates that Zn^{2+} is a tight-binding metal ion cofactor in this enzyme. The apo form of the enzyme displays an identical far-UV CD spectrum, indicating that neither DETAPAC treatment nor Zn^{2+} displacement causes major changes to secondary structure (Figure 5, inset). Zn^{2+} titration of the apo form completely reconstitutes the activity of the enzyme, correlating with a stoichiometry of one Zn^{2+}/mol of enzyme (Figure 5). Further addition of >1 molar equivalent of Zn^{2+} causes inhibition. This Zn^{2+} activation/inhibition profile is very similar to that observed for UDP-3-*O*-(*R*-3-hydroxymyristoyl)-GlcNAc deacetylase (LpxC). It has been proposed that LpxC has two Zn^{2+}-binding sites, one necessary for catalytic activity and a second site with allosteric inhibitory properties [27]. In addition to Zn^{2+},

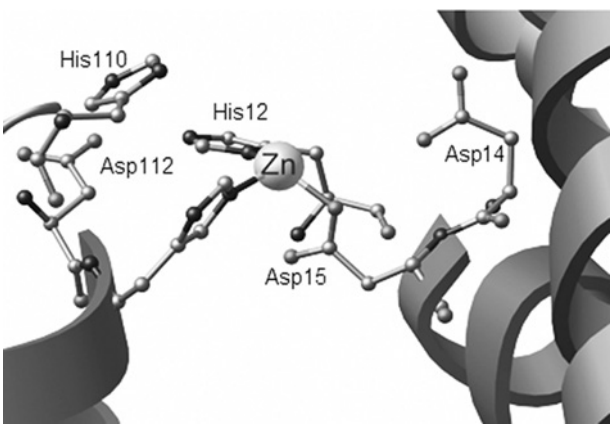

Figure 4 Active-site region of *B. cereus* BC1534 (PDB code 2IXD)

The Zn^{2+} ion is co-ordinated with His^{12}, Asp^{15} and His^{113}.

BA1557 can also be activated upon stoichiometric addition of other metal cations such as Ni^{2+}, Co^{2+} and Fe^{3+} (Supplementary Table S1 at http://www.biochemj.org/bj/454/bj4540239add.htm). These results indicate that BA1557 shares similar profiles for non-specific metal-dependent deacetylation, comparable with the characterized cambialistic behaviours of MshB [28], LpxC [29] and the histone deacetylases [30].

General acid–base catalysis

The pH–activity profile for the BshB reaction with BA1557 presents a bell-shaped curve indicative of general acid–base catalysis [22]. The maximum catalytic activity at subsaturating concentrations of GlcNAc-Mal was reached at pH 7.8. The pH–activity curve fit is consistent with two ionization states with associated pK_a values of 6.5 and 8.5. Interestingly, BA3888 and BC1534 displayed nearly identical pH–activity bell-shaped curves and similar ionization constants (Figure 6A and Table 4). The pH profile of Zn^{2+}- or Co^{2+}-reconstituted BA1557 displayed similar ionization events (Supplementary Figure S5 at http://www.biochemj.org/bj/454/bj4540239add.htm). Likewise,

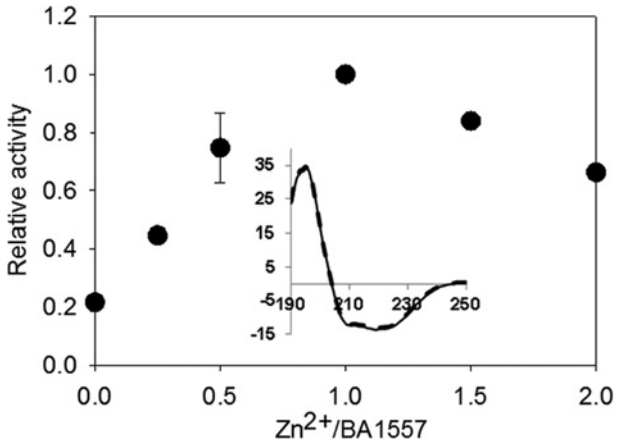

Figure 5 Deacetylation activity of apo-BA1557 reconstituted with different stoichiometric ratios of Zn^{2+}

The preparation and reconstitution of apo-BA1557 were described in the Materials and methods section. The assays were conducted with 0.2 μg of enzyme (0.035 μM) in the presence of 0.25 mM GlcNAc-Mal. The inset panel shows the far-UV CD spectrum of holo-BA1557 (continuous line) and apo-BA1557 (broken line).

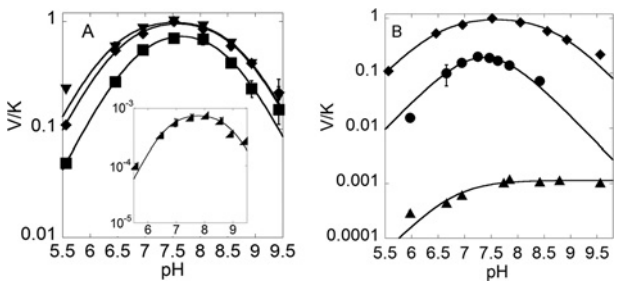

Figure 6 pH–activity profiles of deacetylase enzymes

(**A**) Relative activity (*V*/*K*) of BA1557 (◆), BC1534 (▼), BA3888 (■) and BC3461 (▲, inset). (**B**) Relative activity (*V*/*K*) of BA1557 WT (◆), H110A (●) and D14A (▲). Assays were measured with 0.25 mM GlcNAc-Mal under the pH range 5.97–9.56. All of the pH curves exhibit a bell shape except for D14A which loses the basic limb. The pK_a values were determined by fitting the curve into eqn (1) in the text.

Table 4 pH-dependence of different enzymes/mutants for N-deacetylation of GlcNAc-Mal

Enzyme	pK_a	pK_b
BA1557 (wild-type)	6.50 ± 0.1	8.60 ± 0.2
BA1557 (D14A)	6.82 ± 0.02	–
BA1557 (H110A)	6.66 ± 0.08	8.05 ± 0.04
BA3888	6.82 ± 0.06	8.50 ± 0.05
BC1534	6.58 ± 0.2	8.60 ± 0.02
BC3461	6.64 ± 0.05	8.94 ± 0.04

the pH-dependence on the GlcNAc deacetylation reaction displayed pK_a values of 6.7 and 9.3 (Supplementary Figure S5). These results discard the participation of the malate carboxy group(s) of the substrate or the metal cofactor on either ionization events displayed for this reaction. The similar pH–activity profile of BshB enzymes suggests the participation of conserved residues in the general acid–base catalytic mechanism of the BshB reaction.

Close inspection of the protein environment surrounding the Zn^{2+} cation at the active site of BC1534 (Figure 4) initially suggested His^{110} and Asp^{14} as possible candidates for the general acid and general base respectively. Both residues are strictly conserved in all members of this family of enzymes including the BshB, MshB and Mca sequences (Supplementary Figure S2). ND1 of His^{110} and OD2 of Asp^{14} are located on opposite sides of the acetate group that interacts with Zn^{2+}, approximately 4 Å (1 Å = 0.1 nm) from the metal centre. Individual alanine substitutions of His^{110} and Asp^{14} in BA1557 resulted in decreased activity levels of 4-fold and 3000-fold respectively (Figure 6B and Table 5). The pH–activity profile of H110A BA1557 retained a bell-shaped curve, ruling out the possible participation of this residue as the acid or base in this mechanism. Interestingly, in the structure of BC1534, OD2 of Asp^{112} is located within hydrogen-bonding distance from both NE2 of His^{110} and NE2 of His^{12}, which is a known ligand for the Zn^{2+} (Figure 4). In BC1534, the D112A substitution completely eliminates the GlcNAc deacetylase activity of this enzyme [15]. Unexpectedly, the D14A BA1557 variant retained the ionization event associated with pK_{a1}, but not that for pK_{a2}, suggesting its role as a general acid in the reaction. Although the identity of the general base remains unknown, the pH–activity profile of the D14A variant eliminates the possibility of any dual involvement of this residue, in both ionization events of this reaction mechanism.

Gatekeepers of substrate binding and hydrolysis

The very low catalytic efficiency of the enzyme with GlcNAc compared with GlcNAc-Mal prompted the investigation of substrate analogues where the malate aglycone was replaced by an uncharged methyl or benzyl motif. Table 2 shows that all substrates lacking malate at this position were at least three orders of magnitude less effective as substrates than GlcNAc-Mal. An *in silico* auto-docking approach was used to explore potential binding modes of GlcNAc-Mal with BC1534 [31]. The results from these docking experiments pointed to two arginine residues, Arg^{53} and Arg^{109}, as providing potential electrostatic interactions with the substrate (Supplementary Figure S6 at http://www.biochemj.org/bj/454/bj4540239add.htm). These residues are located on opposite sides of the active site, ~10 Å from each other and ~5 Å from the C1-position of bound acetate, whereas the distances between the Zn^{2+} to the ω-N of Arg^{53} and Arg^{109} were 5.72 Å and 8.03 Å respectively. Interestingly, structural and functional analyses of malate dehydrogenases have shown that two arginine residues (~12 Å apart) are involved in substrate binding providing electrostatic interactions with both carboxy groups of the L-malate substrate [32].

Compared with WT BA1557, an R53A mutation completely eliminated the BshB activity, whereas a more conservative R53K substitution displayed 10^3-fold lower activity for GlcNAc-Mal and no detectable activity with GlcNAc (Table 5 and Supplementary Figure S7 at http://www.biochemj.org/bj/454/bj4540239add.htm). Both substitutions did not impair the secondary structure of this enzyme; the far-UV CD spectrum was nearly identical with that of the WT (Supplementary Figure S4). Sequence alignment of several deacetylases including MshB and Mca indicate that Arg^{53} is strictly conserved. It has been suggested that Arg^{68} and His^{144} of MshB (equivalent to Arg^{53} and His^{110} of BC1534 and BA1557) participate in electrostatic interactions with a sugar hydroxy group of the substrate [26]. Our results with the Arg^{53} mutants provide support for the involvement of this residue in substrate binding. Arg^{109}, however, is only conserved among a group of deacetylases limited to the BshB1 candidates; including BA1557, BC1534 and YpjG (Supplementary Figure S2). The BA1557 R109K variant showed a 6-fold decrease in k_{cat} for GlcNAc-Mal (Table 5 and Supplementary Figure S7). Although

Table 5 Steady-state kinetic parameters of BA1557 variants for N-deacetylation of GlcNAc-Mal

Substrate	Enzyme	K_m (mM)	k_{cat} (s^{-1})	k_{cat}/K_m ($s^{-1}\cdot M^{-1}$)	Relative efficiency
GlcNAc-Mal	Wild-type	0.19 ± 0.03	8.24 ± 0.46	43300 ± 7263	1
	D14A	0.15 ± 0.03	$(2.8 \pm 0.14) \times 10^{-4}$	1.8 ± 0.37	4.1×10^{-5}
	H110A	0.69 ± 0.08	2.19 ± 0.22	3170 ± 486	0.073
	R53A	–*	–*	–*	0
	R53K	0.31 ± 0.05	$(1.4 \pm 0.1) \times 10^{-2}$	45 ± 7.9	1.0×10^{-3}
	R109K	0.24 ± 0.03	1.29 ± 0.16	5380 ± 947	0.124
GlcNAc	Wild-type	57.1 ± 8.5	$(3.3 \pm 0.14) \times 10^{-3}$	0.058 ± 0.010	1
	R53K	–†	–†	–†	0
	R109K	18.6 ± 1.8	$(2.9 \pm 0.1) \times 10^{-3}$	0.16 ± 0.016	2.76
	H110A	–‡	$(0.9 \pm 0.1) \times 10^{-3}$‡	–‡	0

*Assays were performed using 20 μg of enzyme and 0–5 mM GlcNAc-Mal in 50 mM Mops (pH 7.4) at 37 °C.
†Assays were performed in the presence of 20 μg of enzyme and 0–120 mM GlcNAc in 50 mM Mops (pH 7.4) at 37 °C.
‡No substrate saturation was observed up to 180 mM GlcNAc, calculated k_{cat} was based on the velocity at 120 mM.

this substitution impaired the catalytic efficiency of BA1557 with GlcNAc-Mal, the R109K variant showed a modest improvement in reactivity against GlcNAc. This variant enzyme had a lower K_m for GlcNAc (18.6 mM) and similar k_{cat} (2.9×10^{-3} s^{-1}) when compared with the WT constants of 57 mM and 3.3×10^{-3} s^{-1} respectively (Table 5).

Deacetylase enzymes participating in detoxification pathways

BSH is already known to be implicated in some aspect of drug detoxification as exemplified by BST (bacillithiol-S-transferase) (FosB) [16]. A second class of BSTs have also recently been identified, but their target electrophilic substrates are not yet known [13]. On the basis of what has been observed previously in MSH metabolism, enzymes catalysing the BshB reaction (the hydrolysis of GlcNAc-Mal to yield GlcN-Mal) could also potentially be capable of catalysing the hydrolysis of bacillithiol S-conjugates produced in BSH-dependent pathways. The proposed Bca enzyme is thought to be involved in the subsequent step, thus utilizing the products of the BST reaction as substrates. Because of the similarities in mechanism between the BshB and Bca reactions, we have determined the reactivity of BA1557 and BA3888 against BSmB, BSH and BS–Fos. The activity of BA3888 in the hydrolysis of the CysmB side chain of BSmB was 200-fold higher than that of BA1557; however, at 5 mM BSmB the turnover rate of BA3888 was only 1.84 min^{-1} (Table 2). Kinetic analysis of BA1557 and BA3888 with BSH also showed low rates of BSH degradation by formation of cysteine and GlcN, indicating that these enzymes do not contribute to the pool of reduced cysteine levels. Interestingly, the K_m of BA1557 for BSH (0.48 mM) is in the same range as cellular BSH concentrations, suggesting that BSH could act as a feedback inhibitor of this enzyme (Table 3). On the other hand, the BA3888 K_m for BSH was not determined since no substrate saturation was reached up to 5 mM BSH. In our hands, neither BA1557 nor BA3888 showed any detectable activity against BS–Fos. The remarkable selectivity of this group of enzymes for a restricted subset of substrates highlights the importance for *in vivo* screening of candidate compounds in strains lacking these enzymes.

DISCUSSION

In the present study, we performed comparative kinetic analysis of the *B. anthracis* and *B. cereus* deacetylases in performing BshB and Bca reactions to provide biochemical evidence for the cross-functionality of these enzymes in the biosynthesis of BSH. This conclusion supports *in vivo* demonstrations that inactivation of *bshB* in *B. anthracis* and *bshB1* (*ypjG*) in *B. subtilis* decreased, but did not eliminate, the levels of BSH [8]. Kinetic analyses of the BshB reactions with BA1557 and BA3888 show that they display equivalent catalytic efficiencies towards GlcNAc-Mal. However, BA3888 showed a nearly 200-fold higher activity with BSmB compared with BA1557 (Table 2). The reactivity of this enzyme towards larger bacillithiol conjugates provides experimental evidence supporting the role of BA3888 as a catalyst for the Bca reaction. However, it is worth noting that the substrate kinetics for BSmB with BA3888 are still poor and it remains to be seen what the physiologically relevant bacillithiol conjugate substrate(s) is(are) for this enzyme. With BA1557, the very weak amidase activity observed with BSH and a K_m value comparable with its cellular concentration indicates that BSH functions as a feedback inhibitor of this enzyme. However, such feedback inhibition is redundant in the presence of a functional BA3888 enzyme, which can substitute for the GlcNAc-Mal activity of BA1557.

Interestingly, in *S. aureus*, only one BshB-like enzyme has been identified [8]. Among the enzymes described in the present paper, BA3888 is the closest orthologue of *S. aureus* BshB (70/49 % identity/similarity) supporting the notion that a single enzyme in *S. aureus* could fulfil both BshB and Bca functions, although this remains to be proved. Amino acid sequence alignment indicates the presence of a ten-residue insertion (GDPFFANRET in BA3888) in Bca/BshB2 sequences, including BA3888 and *S. aureus* BshB (Supplementary Figure S2A). Although the structural location of sequence is not known, adjacent residues in the BC1534 structure constitute a short loop surrounding the active site. It is possible that this decameric insertion sequence could expand the flexibility of the active site to accommodate potentially larger substrates as in the case of Bca. Nevertheless, the low reactivity of these enzymes against BSmB/BS–Fos suggests the possible occurrence of alternative pathways for detoxification of such adducts and/or the involvement of this group of enzymes in serving as amidases to a specific group of bacillithiol adducts.

Compared with GlcNAc-Mal, the low activity values against GlcNAc, GlcNAc-OMe and GlcNAc-OBn reveals the high degree of specificity for the malate aglycone. Our results from site-directed mutagenesis pointed to BA1557 Arg^{109} as one potential gatekeeper in controlling this specificity or stabilizing a reaction intermediate. Although this model is favoured for BshB enzymes containing arginine residues at positions equivalent to Arg^{109}, this scheme may not apply to all deacetylase enzymes capable of catalysing the BshB reaction (e.g. BA3888 and BC3461 contain valine at the equivalent position). Nonetheless, all four enzymes

tested in the present study showed a high degree of selectivity for GlcNAc-Mal. Controlled substrate binding and hydrolysis may serve as a molecular strategy used by this group of enzymes to restrict the repertoire of physiological substrates.

Functional assignment of residues surrounding Zn^{2+} at the active site confirmed the involvement of Asp^{14} with the second ionization event in the deacetylation mechanism. The abnormally high pK_a of 8.5 is 4 units above the pK_a of free aspartate. Large shifts in aspartate pK_a (>4 units) have been reported for the active-site aspartate residues of human thioredoxin and bacteriorhodopsin [33]. In both cases, the active-site environment surrounding the aspartate side chain favours the protonated acid form during turnover. Studies on the MshB pH–activity profile showed that the rate of deacetylation was also dependent on two ionization events ($pK_{a1} = 7.4$ and $pK_{a2} = 10.5$) [34]. The first ionization event was attributed to Asp^{15} which was proposed to be the general base on this catalytic mechanism. Whereas there is an agreement for the role of Asp^{15} as a general base in the MshB mechanism, the identity of the general acid remains controversial. Solvent isotope effect and site-directed mutagenesis experiments suggest the participation of His^{144} as the general acid [34]; however, pH-dependence studies on H144A MshB [34] and recent structural analysis of this enzyme [35] do not support this model. A previous proposal has evoked the dual role of Asp^{15} as a single general acid and base [26,35]. In this later model, it would be expected that the pK_a associated with the deprotonation of Asp^{15} (pK_{a2}) would be higher than 7.4 (pK_{a1}). In the structure of BA1534 [14], Asp^{14} and His^{110} occupy positions equivalent to Asp^{15} and His^{144} of MshB [26,35]. Interestingly, in the present study, we identified the pK_a associated with Asp^{14} of BA1557 (pK_{a2} of 8.6, Table 3) to be only 1.2 pH units higher than the pK_{a1} of the MshB reaction. Collectively, these results support a mechanism for the BshB reaction involving Asp^{14} as a general acid during the protonation of the nascent amino group on GlcN-Mal product.

The identity of the residue associated with the first ionization event awaits further investigation. Results of the present study rule out the possible participation of His^{110} and Asp^{14} in performing this function. The pH–activity curve of BA1557 using GlcNAc as substrate showed an identical profile eliminating the potential involvement of the malate carboxy groups of the substrate in the first ionization event (Supplementary Figure S5). Alternatively, the activation of a water molecule by the active-site Zn^{2+}, as observed with carbonic anhydrase, or the participation of the Zn^{2+}-co-ordinating Asp^{15} in abstracting the proton from this water, provide possible candidates for the general base in this mechanism. In any event, the conservation of amino acids within the active site imposes a controlled substrate specificity (along with conserved kinetic behaviour) of this group of deacetylases and opens the door for further investigation into their roles in BSH biosynthesis and BSH-mediated xenobiotic detoxification.

AUTHOR CONTRIBUTION

Zhong Fang, Alexandra Roberts, Karissa Weidman and Sunil Sharma performed experiments. Al Claiborne and Patricia Dos Santos conceived the idea, and provided overall direction. Zhong Fang, Christopher Hamilton and Patricia Dos Santos planned experiments, analysed data and wrote the paper. All authors read and approved the content of the paper.

ACKNOWLEDGEMENTS

We thank Vassilis Bouriotis and Vasiliki E. Fadouloglou for the gift of expression plasmids containing BC1534 and BC3461.

FUNDING

Financial support for this work has been provided by a Multidisciplinary Research Grant from the North Carolina Biotechnology Center [grant number M2011-MRG-1116 (to A.C. and P.D.S.)] and the Biotechnology and Biological Sciences Research Council [grant number BB/H013504/1 (to C.J.H)].

REFERENCES

1 Masip, L., Veeravalli, K. and Georgiou, G. (2006) The many faces of glutathione in bacteria. Antioxid. Redox Signaling **8**, 753–762
2 Allocati, N., Federici, L., Masulli, M. and Di Ilio, C. (2009) Glutathione transferases in bacteria. FEBS J. **276**, 58–75
3 Kałuzna, A. and Bartosz, G. (1997) Transport of glutathione S-conjugates in *Escherichia coli*. Biochem. Mol. Biol. Int. **43**, 161–171
4 Jothivasan, V. K. and Hamilton, C. J. (2008) Mycothiol: synthesis, biosynthesis and biological functions of the major low molecular weight thiol in actinomycetes. Nat. Prod. Rep. **25**, 1091–1117
5 Newton, G. L., Buchmeier, N. and Fahey, R. C. (2008) Biosynthesis and functions of mycothiol, the unique protective thiol of *Actinobacteria*. Microbiol. Mol. Biol. Rev. **72**, 471–494
6 Newton, G. L., Av-Gay, Y. and Fahey, R. C. (2000) A novel mycothiol-dependent detoxification pathway in mycobacteria involving mycothiol S-conjugate amidase. Biochemistry **39**, 10739–10746
7 Newton, G. L., Rawat, M., La Clair, J. J., Jothivasan, V. K., Budiarto, T., Hamilton, C. J., Claiborne, A., Helmann, J. D. and Fahey, R. C. (2009) Bacillithiol is an antioxidant thiol produced in Bacilli. Nat. Chem. Biol. **5**, 625–627
8 Gaballa, A., Newton, G. L., Antelmann, H., Parsonage, D., Upton, H., Rawat, M., Claiborne, A., Fahey, R. C. and Helmann, J. D. (2010) Biosynthesis and functions of bacillithiol, a major low-molecular-weight thiol in Bacilli. Proc. Natl. Acad. Sci. U.S.A. **107**, 6482–6486
9 Pother, D., Gierok, P., Harms, M., Mostertz, J., Hochgrafe, F., Antelmann, H., Hamilton, C. J., Borovok, I., Lalk, M., Aharonowitz, Y. and Hecker, M. (2013) Distribution and infection-related functions of bacillithiol in *Staphylococcus aureus*. Int. J. Med. Microbiol. **303**, 114–123
10 Parsonage, D., Newton, G. L., Holder, R. C., Wallace, B. D., Paige, C., Hamilton, C. J., Dos Santos, P. C., Redinbo, M. R., Reid, S. D. and Claiborne, A. (2010) Characterization of the *N*-acetyl-α-D-glucosaminyl L-malate synthase and deacetylase functions for bacillithiol biosynthesis in *Bacillus anthracis*. Biochemistry **49**, 8398–8414
11 Steffek, M., Newton, G. L., Av-Gay, Y. and Fahey, R. C. (2003) Characterization of *Mycobacterium tuberculosis* mycothiol S-conjugate amidase. Biochemistry **42**, 12067–12076
12 Rawat, M., Kovacevic, S., Billman-Jacobe, H. and Av-Gay, Y. (2003) Inactivation of mshB, a key gene in the mycothiol biosynthesis pathway in *Mycobacterium smegmatis*. Microbiology **149**, 1341–1349
13 Newton, G. L., Fahey, R. C. and Rawat, M. (2012) Detoxification of toxins by bacillithiol in *Staphylococcus aureus*. Microbiology **158**, 1117–1126
14 Fadouloglou, V. E., Deli, A., Glykos, N. M., Psylinakis, E., Bouriotis, V. and Kokkinidis, M. (2007) Crystal structure of the BcZBP, a zinc-binding protein from *Bacillus cereus*. FEBS J. **274**, 3044–3054
15 Deli, A., Koutsioulis, D., Fadouloglou, V. E., Spiliotopoulou, P., Balomenou, S., Arnaouteli, S., Tzanodaskalaki, M., Mavromatis, K., Kokkinidis, M. and Bouriotis, V. (2010) LmbE proteins from *Bacillus cereus* are de-N-acetylases with broad substrate specificity and are highly similar to proteins in *Bacillus anthracis*. FEBS J. **277**, 2740–2753
16 Roberts, A. A., Sharma, S. V., Strankman, A. W., Duran, S. R., Rawat, M. and Hamilton, C. J. (2013) Mechanistic studies of FosB: a divalent metal-dependent bacillithiol-S-transferase that mediates fosfomycin resistance in *Staphylococcus aureus*. Biochem. J. **451**, 69–79
17 Sharma, S. V., Jothivasan, V. K., Newton, G. L., Upton, H., Wakabayashi, J. I., Kane, M. G., Roberts, A. A., Rawat, M., La Clair, J. J. and Hamilton, C. J. (2011) Chemical and chemoenzymatic syntheses of bacillithiol: a unique low-molecular-weight thiol amongst low G + C Gram-positive bacteria. Angew. Chem. Int. Ed. **50**, 7101–7104
18 Yeager, A. R. and Finney, N. S. (2005) Synthesis of fluorescently labeled UDP-GlcNAc analogues and their evaluation as chitin synthase substrates. J. Org. Chem. **70**, 1269–1275
19 Ma, Z., Zhang, J. and Kong, F. (2004) Synthesis of two oligosaccharides, the GPI anchor glycans from *S. cerevesiae* and *A. fumigatus*. Carbohydr. Res. **339**, 29–35
20 Bradford, M. M. (1976) A rapid and sensitive method for the quantitation of microgram quantities of protein utilizing the principle of protein-dye binding. Anal. Biochem. **72**, 248–254
21 Anderberg, S. J., Newton, G. L. and Fahey, R. C. (1998) Mycothiol biosynthesis and metabolism: cellular levels of potential intermediates in the biosynthesis and degradation of mycothiol in *Mycobacterium smegmatis*. J. Biol. Chem. **273**, 30391–30397

22 McClerren, A. L., Zhou, P., Guan, Z., Raetz, C. R. and Rudolph, J. (2005) Kinetic analysis of the zinc-dependent deacetylase in the lipid A biosynthetic pathway. Biochemistry **44**, 1106–1113
23 Selbach, B., Earles, E. and Dos Santos, P. C. (2010) Kinetic analysis of the bisubstrate cysteine desulfurase SufS from *Bacillus subtilis*. Biochemistry **49**, 8794–8802
24 Huang, X. and Hernick, M. (2010) A fluorescence-based assay for measuring *N*-acetyl-1-D-*myo*-inosityl-2-amino-2-deoxy-α-D-glucopyranoside deacetylase activity. Anal. Biochem. **414**, 278–281
25 Hernick, M. (2011) Fluorescence-based methods to assay inhibitors of lipopolysaccharide synthesis. Methods Mol. Biol. **739**, 123–133
26 Maynes, J. T., Garen, C., Cherney, M. M., Newton, G., Arad, D., Av-Gay, Y., Fahey, R. C. and James, M. N. (2003) The crystal structure of 1-D-*myo*-inosityl 2-acetamido-2-deoxy-α-D-glucopyranoside deacetylase (MshB) from *Mycobacterium tuberculosis* reveals a zinc hydrolase with a lactate dehydrogenase fold. J. Biol. Chem. **278**, 47166–47170
27 Jackman, J. E., Raetz, C. R. and Fierke, C. A. (1999) UDP-3-*O*-(*R*-3-hydroxymyristoyl)-*N*-acetylglucosamine deacetylase of *Escherichia coli* is a zinc metalloenzyme. Biochemistry **38**, 1902–1911
28 Huang, X., Kocabas, E. and Hernick, M. (2011) The activity and cofactor preferences of *N*-acetyl-1-D-*myo*-inosityl-2-amino-2-deoxy-α-D-glucopyranosi deacetylase (MshB) change depending on environmental conditions. J. Biol. Chem. **286**, 20275–20282
29 Gattis, S. G., Hernick, M. and Fierke, C. A. (2010) Active site metal ion in UDP-3-*O*-((*R*)-3-Hydroxymyristoyl)-*N*-acetylglucosamine deacetylase (LpxC) switches between Fe(II) and Zn(II) depending on cellular conditions. J. Biol. Chem. **285**, 33788–33796
30 Dowling, D. P., Gattis, S. G., Fierke, C. A. and Christianson, D. W. (2010) Structures of metal-substituted human histone deacetylase 8 provide mechanistic inferences on biological function. Biochemistry **49**, 5048–5056
31 Trott, O. and Olson, A. J. (2009) AutoDock Vina: improving the speed and accuracy of docking with a new scoring function, efficient optimization, and multithreading. J. Comput. Chem. **31**, 455–461
32 Bell, J. K., Yennawar, H. P., Wright, S. K., Thompson, J. R., Viola, R. E. and Banaszak, L. J. (2001) Structural analyses of a malate dehydrogenase with a variable active site. J. Biol. Chem. **276**, 31156–31162
33 Turner, G. J. (2008) Mutagenic analysis of membrane protein functional mechanisms: bacteriorhodopsin as a model example. Methods Cell Biol. **84**, 479–515
34 Huang, X. and Hernick, M. (2012) Examination of mechanism of *N*-acetyl-1-D-*myo*-inosityl-2-amino-2-deoxy-α-D-glucopyranosi de deacetylase (MshB) reveals unexpected role for dynamic tyrosine. J. Biol. Chem. **287**, 10424–10434
35 Broadley, S. G., Gumbart, J. C., Weber, B. W., Marakalala, M. J., Steenkamp, D. J. and Sewell, B. T. (2012) A new crystal form of MshB from *Mycobacterium tuberculosis* with glycerol and acetate in the active site suggests the catalytic mechanism. Acta Crystallogr., Sect. D: Biol. Crystallogr. **68**, 1450–1459

Received 20 March 2013/6 June 2013; accepted 11 June 2013
Published as BJ Immediate Publication 11 June 2013, doi:10.1042/BJ20130415

Biochem. J. (2013) **454**, 239–247 (Printed in Great Britain) doi:10.1042/BJ20130415

online data

SUPPLEMENTARY ONLINE DATA

Cross-functionalities of *Bacillus* deacetylases involved in bacillithiol biosynthesis and bacillithiol-S-conjugate detoxification pathways

Zhong FANG*, Alexandra A. ROBERTS†, Karissa WEIDMAN*, Sunil V. SHARMA†, Al CLAIBORNE‡, Christopher J. HAMILTON† and Patricia C. DOS SANTOS*[1]

*Department of Chemistry, Wake Forest University, Winston-Salem, NC 27109, U.S.A., †School of Pharmacy, University of East Anglia, Norwich Research Park, Norwich NR4 7TJ, U.K., and ‡Center for Structural Biology, Wake Forest University School of Medicine, Winston-Salem, NC 27109, U.S.A.

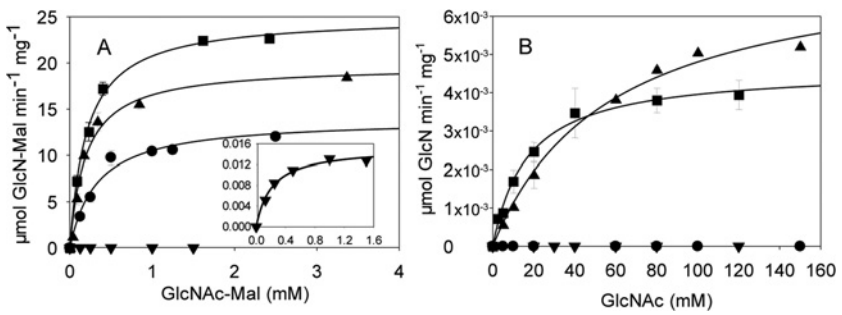

Figure S1 Substrate saturation curves of BA1557 (▲), BC1534 (■), BA3888 (●) and BC3461 (▼) with GlcNAc-Mal (A) and GlcNAc (B) as substrates

Assays were performed with GlcNAc-Mal (0–3.36 mM) and GlcNAc (0–150 mM) at fixed concentrations of deacetylases as described in the Materials and methods section of the main text.

Table S1 Activity of BA1557 upon reconstitution with different metals

Assay was performed with 0.2 μg of apo-BA1557 reconstituted with one stoichiometric ratio of different metal ion in the presence of 0.25 mM GlcNAc-Mal.

Metal ion	Velocity (μmol/min per mg)	Relative activity
Apo (<5 %)	1.5 ± 0.3	0.20
Fe^{3+}	7.1 ± 0.2	0.95
Co^{2+}	11.3 ± 1.1	1.50
Zn^{2+}	7.5 ± 0.4	1.00
Ni^{2+}	22.6 ± 9.6	3.01
Mg^{2+}	3.0 ± 0.1	0.40
Ca^{2+}	14.3 ± 3.4	1.91

[1] To whom correspondence should be addressed (email dossanpc@wfu.edu).

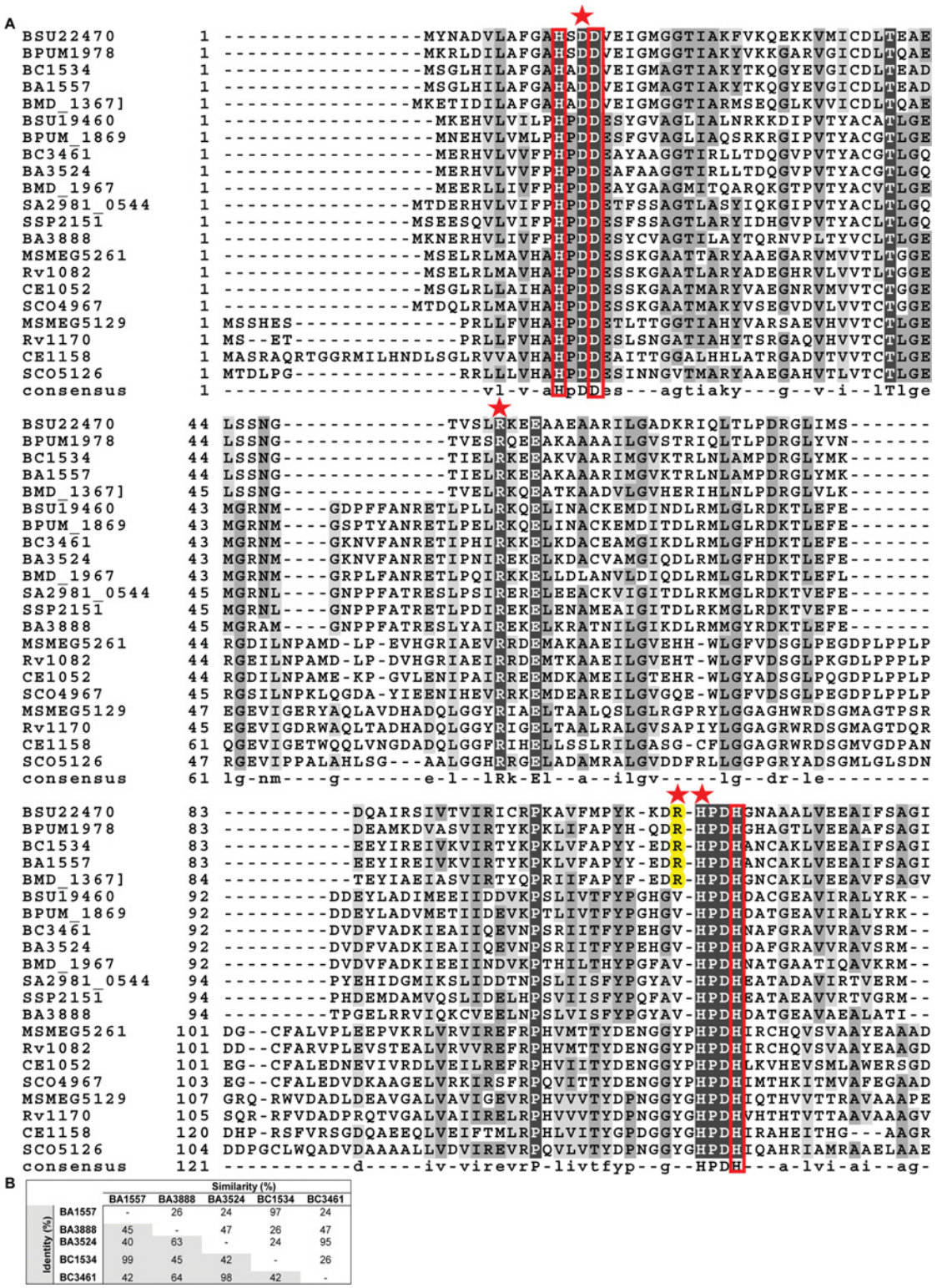

Figure S2 Sequence alignment of deacetylases

(**A**) Amino acid sequence alignment of deacetylase enzymes. ClustalW alignment using Gonnet series matrix including deacetylase sequences from *B. anthracis* str. Ames (BA1557, BA3888 and BA3524), *B. cereus* ATCC 14579 (BC1534 and BC3461), *B. subtilis* subsp. *subtilis* str. 168 (BSU22470 and BSU19460), *B. pumilus* SAFR-032 (BPUM1978 and BPUM_1869), *B. megaterium* DSM 319 (BMD_1367 and BMD_1967), *S. aureus* 04-02981 (SA2981_0544), *S. saprophyticus* subsp. *saprophyticus* ATCC 15305 (SSP2151), *M. smegmatis* str. MC2 155 (MSMEG5261 and MSMEG5129), *Mycobacterium tuberculosis* H37Rv (Rv1082 and Rv1170), *Corynebacterium efficiens* YS-314 (CE1052 and CE1158) and *Streptomyces coelicolor* A3(2) (SCO4967 and SCO5126). Shown is the N-terminal portion of the sequence alignment with completely conserved residues shaded in dark grey with white font, identical residues shaded in grey and similar residues in light grey. Residues co-ordinating the Zn^{2+} ion in the structures of BshB1 (BC1534) and MshB1 (Rv1170) are indicated with a red box. Residues investigated in the present study are indicated with a red star. Arg^{109} proposed to be involved in substrate binding and hydrolysis in BshB1 sequences is highlighted in yellow. Alignment was constructed in Biology Workbench. (**B**) Sequence identity (grey boxes) and similarity (white boxes) between the N-deacetylase enzymes analysed in the present study from *B. anthracis* str. Ames and *B. cereus* ATCC-14579.

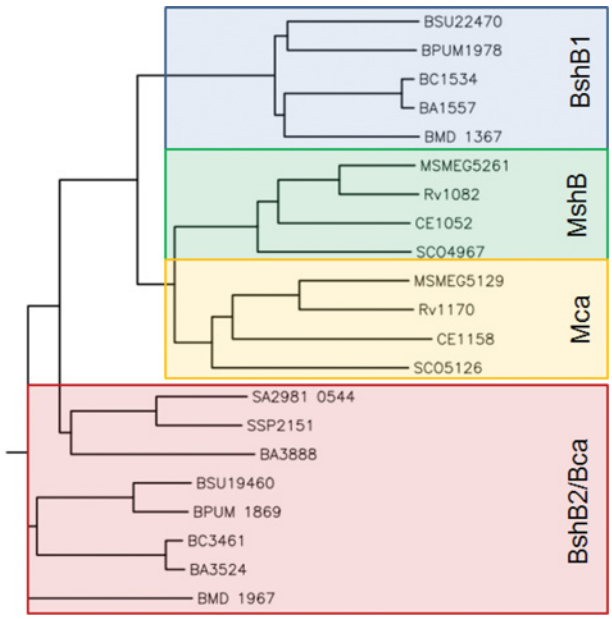

Figure S3 Drawgram of deacetylase enzymes included in Figure S1A

PHYLIP rooted phylogenetic tree phenogram (Drawgram) constructed in Biology Workbench depicts the phylogenetic distribution of deacetylases. The shaded boxes indicate proposed functional assignments for deacetylase candidate sequences.

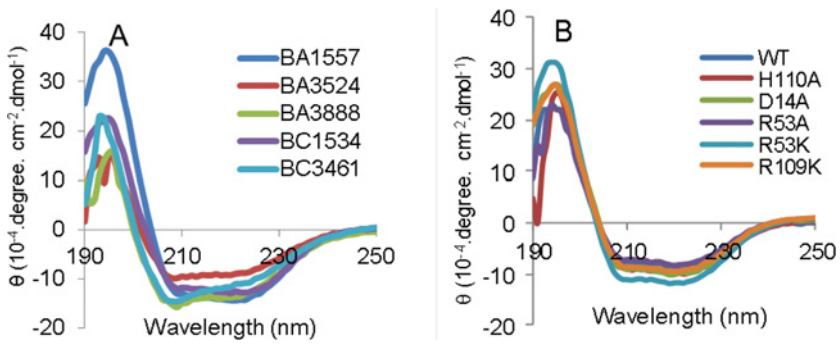

Figure S4 Far-UV CD spectra of deacetylases BA1557, BC1534, BA3888, BC3461 and BA3524 (A) and BA1557 variants H110A, D14A, R53A, R53K and R109K (B)

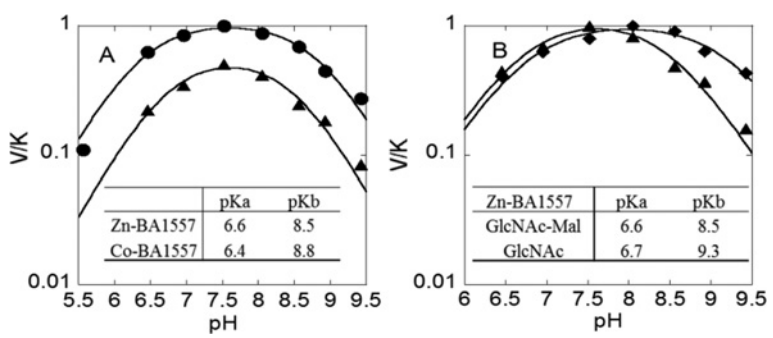

Figure S5 pH–activity profiles of deacetylase activity of BA1557

(**A**) Relative activity (V/K) of Co^{2+}-BA1557 (●) and Zn^{2+}-BA1557 (▲) using GlcNAc-Mal as substrate. (**B**) Relative activity (V/K) of Zn^{2+}-BA1557 with GlcNAc-Mal (▲) and GlcNAc (◆) as substrates. Assays were measured with 0.25 mM GlcNAc-Mal or 50 mM GlcNAc under the pH range 5.5–9.5. The line is the best fit of eqn (1) as described in the Materials and methods section of the main text. pK_a and pK_b are shown in the inset.

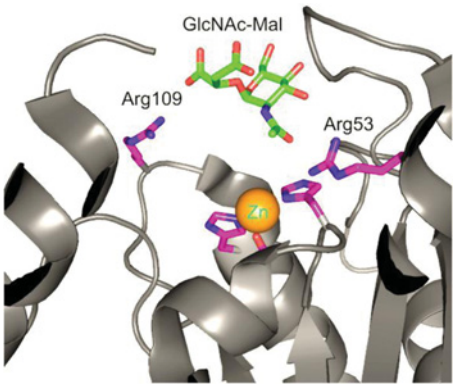

Figure S6 Model of the active site of BC1534 (PDB code 2IXD) in complex with GlcNAc-Mal

The GlcNAc-Mal molecule was generated by Gaussian09 to achieve the most stable conformation. The model is the result of a simulated annealing docking of GlcNAc-Mal to BC1534 using Autodock Vina [31]. Arg^{53} and Arg^{109} on each site of the catalytic Zn^{2+} with a distance 6.17 and 2.39 Å respectively are shown. These residues locate in a position which has ~4.5 Å from the carboxy groups of the malate moiety.

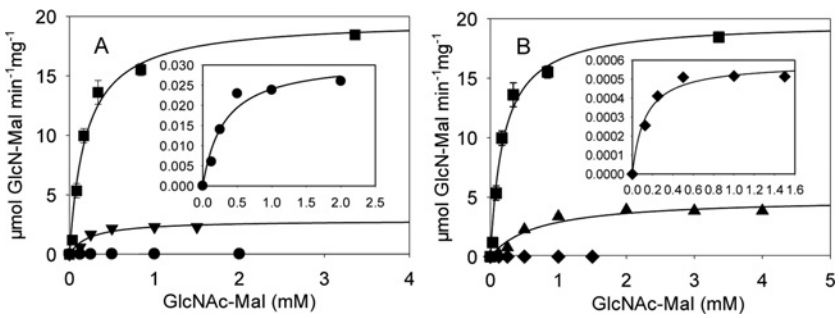

Figure S7 Kinetic analysis of BA1557 variants

(**A**) BA1557 WT (■), 109K (▼) and R53K (●). (**B**) BA1557 WT (■), H110A (▲) and D14A (◆). The initial rates for the deacetylation of GlcNAc-Mal (0–3.36 mM) were measured by the slopes of four-time point during a 30 min reaction for WT and R109K and a 3 h reaction for R53K.

Received 20 March 2013/6 June 2013; accepted 11 June 2013
Published as BJ Immediate Publication 11 June 2013, doi:10.1042/BJ20130415